ACS Sensors

Article

Cite This: ACS Sens. 2018, 3, 1838−1845

pubs.acs.org/acssensors

A Fluorescent Carbon Nanotube Sensor Detects the Metastatic Prostate Cancer Biomarker uPA

Ryan M. Williams,[†] Christopher Lee,[†] and Daniel A. Heller*[,†,‡]

[†]Memorial Sloan Kettering Cancer Center, New York, New York 10065, United States

[‡]Weill Cornell Medicine, New York, New York 10065, United States

Supporting Information

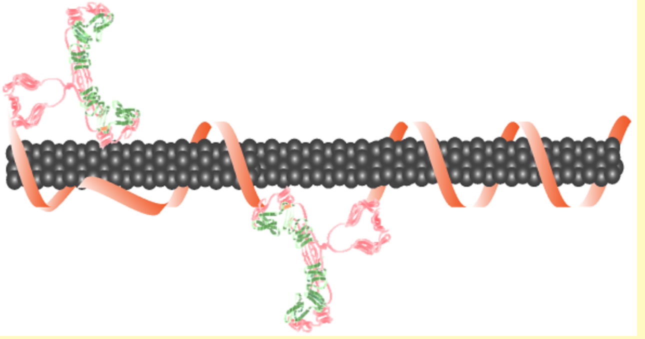

ABSTRACT: Therapeutic outcomes in patients with prostate cancer are hindered by the inability to discern indolent versus aggressive disease. To address this problem, we developed a quantitative fluorescent nanosensor for the cancer biomarker urokinase plasminogen activator (uPA). We used the unique fluorescent characteristics of single-walled carbon nanotubes (SWCNT) to engineer an optical sensor that responds to uPA via optical bandgap modulation in complex protein environments. The sensing characteristics of this construct were modulated by passivation of the hydrophobic SWCNT surface with bovine serum albumin (BSA). The sensor enabled quantitative detection of known uPA concentrations in human blood products. These experiments potentiate future use of this technology as a rapid, point-of-care sensor for biomarker measurements in patient fluid samples. We expect that further work will develop a method to discern aggressive vs indolent prostate cancer and reduce overtreatment of this disease.

KEYWORDS: *biosensor, optical sensor, protein, nanocarbon, nanomedicine, prostatic carcinoma*

Prostate cancer is the most-diagnosed non-skin cancer among males in the United States and accounts for the second greatest number of cancer-related deaths in this population.[1] The current standard of practice for disease detection is through a digital rectal exam and by measuring the serum biomarker prostate specific antigen (PSA).[2] However, in up to 85% of cases, these metrics give contradictory results.[2] PSA-based detection has an up to 76% false-positive rate, fails to find early stage disease, and does not significantly affect outcomes in most men.[3−5] For these reasons, the U.S. Preventative Services Task Force recommends against its use in most circumstances, though the test continues to be used.[4,6,7] Thus, additional diagnostic methods to supplement traditional PSA-based detection would benefit this patient population.

Coupled with the problems of sensitivity and specificity, current diagnostic methods fail to differentiate aggressive versus indolent prostate cancer.[8,9] Therefore, men who are diagnosed with prostate cancer but would not exhibit symptoms in their lifetime, defined as overdiagnoses, are overtreated.[10−12] It is therefore necessary to identify patient populations that have diagnosable prostate cancer that would not progress to aggressive, metastatic disease.

Among potential biomarkers that have the potential to distinguish aggressive, metastatic prostate cancer from indolent disease, urokinase plasminogen activator (uPA) is a promising option. Intratumoral levels of uPA correlate with poor patient prognosis for multiple cancer types,[13] are predictive of therapeutic regimen efficacy, and are predictive of future metastatic development.[14−16] Serum levels of uPA correlate well with the presence of metastatic disease.[17,18] Preoperative prostate cancer patients with local lymph invasion and skeletal metastases had significantly greater serum uPA levels (2−5 times more) than did healthy patients or compared to those that did not have extraprostatic invasion.[17,18] Furthermore, uPA has greater prognostic and metastatic predictive value than more traditional serum-based markers.[18,19] Thus, uPA may serve as a supplemental biomarker to differentiate aggressive from indolent prostate cancer.

Prior work has used the unique properties of nanomaterials to achieve detection of protein biomarkers. For example, studies have developed such sensors for blood-based detection using the surface-enhanced Raman scattering (SERS) and plasmonic properties of gold nanoparticles.[20,21] Other work has used the electrochemical properties of carbon nanotubes to report protein biomarker detection.[22,23]

The near-infrared (NIR) photoluminescence (fluorescence) of single-walled carbon nanotubes (SWCNTs) has been investigated for optical imaging and biosensing applications. This fluorescence, in the 900−1600 nm range, is highly penetrant to living tissue and fluids[24−26] and is uniquely photostable.[27] In addition, SWCNT fluorescence is extremely

Received: July 11, 2018
Accepted: August 21, 2018
Published: August 31, 2018

DOI: 10.1021/acssensors.8b00631
ACS Sens. 2018, 3, 1838−1845

sensitive to its local environment, wherein the fluorescence intensity or energy can be modulated due to solvatochromic, redox, or Coulombic effects.[28−31,34] Prior work has found that changes in the local dielectric environment of the nanotube[29,32,33] or a change in its local electrostatic environment[28,34−37] can alter nanotube emission energy (wavelength) through bandgap modulation.[33] Using these properties, carbon nanotubes have been employed as an optical transducer element for the detection of multiple classes of analytes, in vitro, ex vivo, and in vivo,[33,35,36] including protein biomarkers of cardiac function in vitro, and ovarian cancer in vivo[38,39]

In this work, we used the optical properties of carbon nanotubes to develop a sensitive and specific sensor for the metastatic prostate cancer biomarker uPA. Photoluminescent SWCNTs were engineered to specifically respond to uPA via antibody conjugation, which results in modulation of the optical bandgap following analyte interaction. We investigated the mechanism of sensing for this sensor and used these properties to detect the presence of uPA in whole blood, serum, and plasma.

■ EXPERIMENTAL SECTION

Sensor Synthesis. We suspended HiPCO single-walled carbon nanotubes (SWCNT) (Unidym; Sunnyvale, CA) with single-stranded $(TAT)_6$ DNA modified with a 3′ primary amine, in PBS, using a procedure adapted from a previous protocol.[40] We used a 2:1 mass ratio of ssDNA to dry nanotubes in a 1 mL volume of PBS, sonicating for 30 min at approximately 13 W (Sonics & Materials, Inc.; Newtown, CT). We then ultracentrifuged the suspension for 30 min at 280,000*g*, removing the top 75% of the solution for further processing. 100 kDa MWCO centrifugal filters (Millipore; Billerica, MA) were used to remove excess ssDNA by centrifugation at 15,000*g* for 7 min and one wash with PBS with the same parameters. We determined ssDNA-SWCNT concentration using UV/vis/nIR spectroscopy (Jasco V-670; Tokyo, Japan) using the extinction coefficient Abs_{630} = 0.036 L mg^{-1} cm^{-1}.

The ssDNA-SWCNT suspension was chemically conjugated using carbodiimide chemistry to a mouse monoclonal IgG_1 anti-uPA antibody (PGM2001; Santa Cruz Biotechnology; Dallas, TX). We used 1-ethyl-3-(3-dimethylainopropyl)carbodiimide (EDC) and *N*-hydroxysuccinimide (NHS) in a 10× and 25× molar excess, respectively, to activate the carboxylic acids of the antibody and quenched the reaction with 1.4 μL 2-mercaptoethanol. The activated antibody was added to ssDNA-SWCNT in an equimolar ratio to the ssDNA for 2 h on ice. The solution was dialyzed against water in a 1 MDa MWCO filter at 4 °C for 48 h to remove excess reagents. Absorbance spectra and near-infrared photoluminescence (PL) plots were obtained to confirm complex stability and measure optical properties. Dynamic light scattering (DLS) was performed (Malvern; Worcestershire, United Kingdom) to determine the relative size of nanotube complexes by their correlation coefficient, with larger coefficients relating to larger particles. Electrophoretic light scattering (ELS) was performed with the same instrument to determine the average charge (three measurements each) of the ssDNA-SWCNT and Ab-ssDNA-SWCNT constructs.

Fluorescence Spectroscopy. Near-infrared fluorescence emission spectra from the nanotube complexes were acquired in solution using a home-built optical apparatus.[41] This setup involves excitation using either a 1 W continuous-wave 730 nm laser (Frankfurt Laser Company; Friedrichsdorf, Germany) or a tunable white light SuperK EXTREME laser source (NKT Photonics; Birkerod, Denmark). Each source was fed into an inverted IX-71 microscope (Olympus; Tokyo, Japan) and passed through a 20× NIR objective (Olympus). The light illuminated a 100 μL sample in a UV half area 96 well plate (Corning; Corning, NY). Fluorescence emission was collected back through the 20× objective, passed through an 875 nm dichroic mirror, and f/# matched to the spectrometer before injecting into an IsoPlane spectrograph with a 410 μm slit width (Princeton Instruments; Trenton, NJ). A 86 g/mm grating with 950 nm blaze wavelength was used to disperse emission in the spectral range of 930−1369 nm with a ∼0.7 nm resolution. We used a PIoNIR InGaAs 640 × 512 pixel array (Princeton Instruments) to collect the emission. Excitation/emission plots were gathered using the supercontinuum laser source and a VARIA bandpass filter in 3 nm steps from 500−827 nm. A halogen calibration light source, HL-3-CAL EXT (Ocean Optics; Dunedin, FL), was used to correct for excitation power, spectrometer, detector, and optics wavelength-dependent features. A Hg/Ne calibration lamp was used to calibrate spectrometer wavelength. Background subtraction was performed using another well in the same plate using identical buffer/serum conditions as the investigated sample. Custom MATLAB code (MathWorks; Natick, MA) was used to apply spectral correction, background subtraction, and fitting of all nanotube chirality emission peaks to Lorentzian functions. MATLAB code is available upon request.

Sensor Characterization. To test the response to uPA, we diluted the sensor complex to a concentration of 0.5 mg/L in PBS in a 100 μL total volume in a 96-well plate. In triplicate, the following concentrations of recombinant human uPA (Ser21-Leu431; RayBiotech; Norcross, GA) were added to the sensor: 0.1, 1, 5, 10, 25, 50, 100, 150, 200, and 250 nM uPA, as well as a control with no uPA added. Data were obtained as described above for 3 h in 30 min increments. For experiments performed with BSA coating, a 50× BSA:SWCNT mass ratio of bovine serum albumin (Sigma-Aldrich; St. Louis, MO) was added to the nanotube stock on ice for 30 min prior to incubation with uPA. For experiments performed in serum, the BSA-coated or uncoated nanotubes were added to a solution of 10% fetal bovine serum (Gibco; New York, NY) in PBS prior to uPA addition. The same concentration ranges were used in all conditions to ensure accuracy of comparisons across experiments.

Each sample was exposed to the 730 nm excitation laser for three seconds to acquire individual spectra, as described above. Emission bands were fit to Lorentzian functions, as described above. The three chiralities with the greatest intensities, and therefore strongest fits, were chosen for characterization. Determination of sensor parameters was performed using the change from unchallenged control sensor of each average center wavelength in triplicate wells for each of three nanotube chiralities: (9,4), (8,6), and (8,7). The limit of detection was defined as the lowest concentration of uPA tested at which the change from control was larger than the standard deviation of the three measurements. Sensor dissociation constant (K_d) was obtained by fitting the wavelength change from control data for all data points to a standard model of noncooperative saturation single-site specific binding kinetics with the equation: $Y = B_{max} \times X/(K_d + X)$, wherein B_{max} is the maximum specific binding as measured by wavelength change in nm and K_d is the equilibrium binding constant in nM. Goodness of fit was determined by R^2 values. All R^2 values reached at least 0.78, signifying a strong correlation.[42,43] The maximum red-shift was the largest average change found in a set of experiments.

Sensor Function in Human Samples. To test sensor functionality in various human blood products, we performed near-infrared fluorescence spectroscopy similar to above. In each experiment, the sensor was added to 0.5 mg/L in a final volume of 100 μL in a 96-well plate. Human blood products were obtained retrospectively from adult donors without a cancer diagnosis after obtaining informed consent on MSKCC IRB# 06−107. An initial experiment was performed with the BSA-coated sensor in a solution of 10% human whole blood in PBS where either a final concentration of 100 nM uPA was added or not and measured 60 min post-addition. The change resulting from uPA addition was measured by a shift in the fluorescence emission band of the (9,4), (8,6), and (8,7) nanotube chiralities. Additional experiments were performed where a solution of either 10% human heparinized plasma, human ethylenediaminetetraacetic acid (EDTA) plasma, or 10% human serum in PBS was added to the sensor with a final concentration of 100 nM uPA, or 0 nM control, in triplicate. Fluorescence spectroscopy was conducted 30, 90, 120, and 150 min post-addition.

DOI: 10.1021/acssensors.8b00631
ACS Sens. 2018, 3, 1838−1845

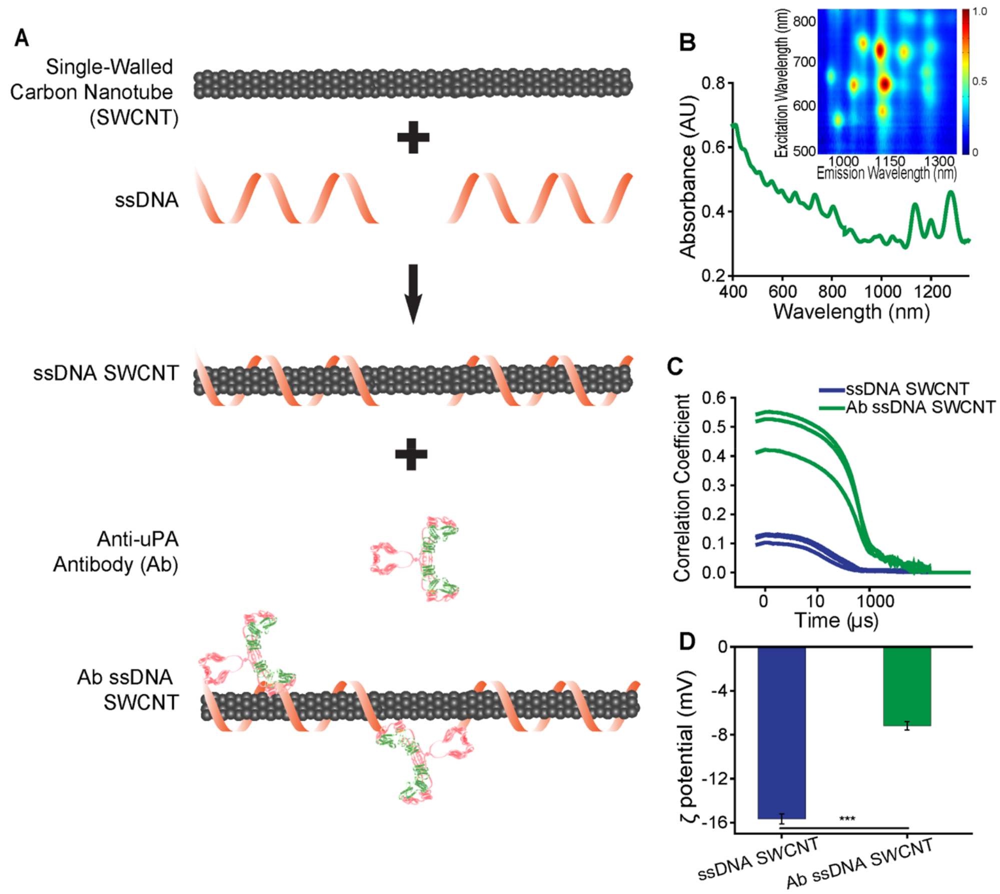

Figure 1. Synthesis and characterization of Anti-uPA-DNA-SWCNT complexes. (A) Scheme of Ab ssDNA SWCNT sensor complex synthesis. (B) Absorbance spectrum of the sensor complexes. Inset: Photoluminescence (PL) excitation/emission plot of the Anti-uPA-DNA-SWCNT complex. (C) Correlogram from dynamic light scattering measurements of pre- and post-Ab-conjugated ssDNA SWCNT complexes. Three measurements for each complex are shown. (D) Electrophoretic light scattering of ssDNA SWCNT before and after anti-uPA antibody conjugation. Each bar represents mean of three measurements ± SD *** = $p < 0.001$; t test.

■ RESULTS AND DISCUSSION

We developed an optical sensor for the biomarker uPA to allow for rapid solution-based measurements. The nanosensor complexes were synthesized from single-walled carbon nanotubes encapsulated with single-stranded DNA $(TAT)_6$ modified via a 3′ primary amine functional group that was conjugated to a monoclonal anti-uPA antibody (Figure 1A). Absorbance and photoluminescence emission/excitation spectra were collected to assess the optical properties of the complexes. The spectra exhibited characteristic bandwidths and intensities of colloidally stable single-walled carbon nanotubes[44] (Figure 1B). Using dynamic light scattering (DLS), we measured changes in particle sizes upon conjugation of the suspended DNA-nanotube complexes with the uPA antibody (Figure 1C). We found that particle sizes became larger, as defined by shifts in the autocorrelation function, suggesting successful complexation of the antibodies with the nanotubes to result in a larger Anti-uPA-DNA-SWCNT complex. We also found a decrease in ζ-potential of the complexes via electrophoretic light scattering (ELS) (Figure 1D), an expected result in light of prior studies,[44−46] further suggestion successful antibody conjugation.

To assess the sensitivity and dynamic range of this sensor, we added increasing concentrations of uPA to the Anti-uPA-DNA-SWCNT sensor complexes in phosphate-buffered saline (PBS). Ten concentrations of uPA ranging from 100 pM to 250 nM were added in triplicate to the sensor in solution. Near-infrared (900−1400 nm) photoluminescent emission was collected following 730 nm excitation of the sensor.[41] The change in fluorescence emission wavelength was assessed for multiple nanotube chiralities in this range. We observed red-shifting of the (9,4) nanotube chirality in response to uPA concentrations between 25 and 100 nM, compared to control, with a maximum red-shift of 1.6 nm (Figure 2A). The sensor exhibited a limit of detection (LOD) of 50 nM uPA and a dissociation constant (K_d) of 100.05 nM (Figure S1A). We additionally observed red-shifting of the (8,6) chirality up to 4.2 nm and (8,7) chirality up to 3.1 nm (Figure S2A,B). We attribute the emission red-shifting to an increase in the local electrostatic charge density on the nanotube due to localization of the uPA near the nanotube surface. This is suggested by our previous findings wherein charged polyelectrolytes result in red-shifting of the nanotube emission bands.[34−37] Furthermore, structural studies of the uPA protein find multiple charged surface moieties.[47] The binding of uPA to the antibody-DNA-nanotube complex likely sequesters the uPA near the surface of the nanotube to promote static charge accumulation.

We then investigated the response of the sensor to increasing concentrations of uPA in 10% fetal bovine serum (FBS) to simulate the complex protein environment of clinical biosensors. FBS specifically, and serum in general, is composed

DOI: 10.1021/acssensors.8b00631
ACS Sens. 2018, 3, 1838−1845

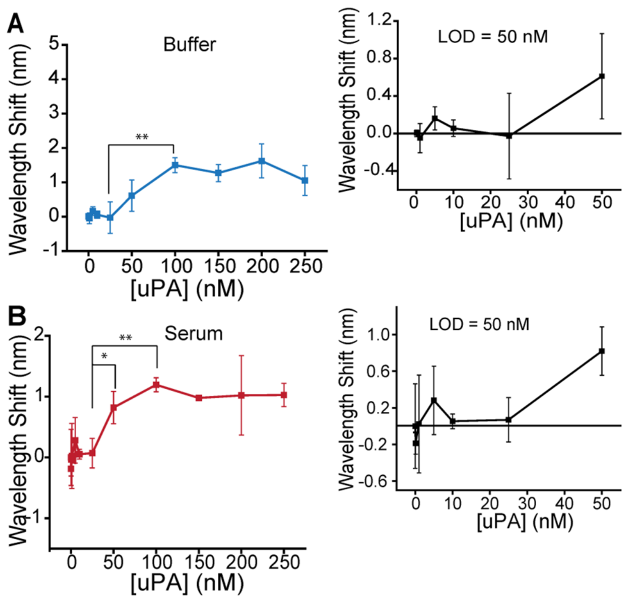

Figure 2. Antibody-SWCNT uPA sensor response. (A) Change in sensor emission center wavelength in PBS as a function of uPA concentration compared to control. Positive value signifies a red-shift of the (9,4) nanotube chirality. Two-sided one-way ANOVA with Tukey posthoc analysis performed to determine significance within the dynamic range of the sensor (25−100 nM): ** = 25 nM and 100 nM (p = 0.0075); other comparisons are not significant. (B) Change in sensor fluorescence emission center wavelength in 10% FBS as a function of uPA concentration added for the (9,4) nanotube chirality. Two-sided one-way ANOVA with Tukey posthoc analysis performed to determine significance within the dynamic range of the sensor (25−100 nM): ** = 25 nM and 100 nM (p = 0.0018); * = 25 nM and 50 nM (p = 0.013); other comparisons are not significant. Points represent the mean ± SD of three experiments. The low-concentration region on the left is magnified on the right to clearly elucidate the limit of detection of the sensor under these conditions.

of many proteins, including albumin which is the most abundant, antibodies, and other signaling proteins, among others. It is also composed of many other interferents, including small molecules such as steroids, ions, and lipids, among others. Equivalent concentrations of uPA as above were added in triplicate to the sensor in FBS and fluorescence emission wavelength was assessed as before. Again, we observed red-shifting between 25 and 100 nM, and while the LOD was 50 nM (Figure 2B), analogous to the sensor in buffer, the maximum red-shift was only 1.2 nm, just 75% of the response without serum. We also observed a K_d of 58.24 nM (Figure S1C) and similar characteristics for the (8,6) and (8,7) chiralities, with red-shifts of 1.5 and 2.3 nm and dissociation constants of 29.9 nM and 42.8 nM, respectively (Figure S2C,D). Thus, as expected, serum caused a decrease in sensor functionality due to the effects of nonspecific interferent adsorption to the surface of the nanotube and a reduction in diffusivity of the target uPA, hindering its interaction with the antibody.

To increase the sensitivity and specificity of the sensor, we investigated passivation of the nanotube surface with bovine serum albumin (BSA). Albumin protein is used for its ability to prevent nonspecific protein adsorption to surfaces for various applications.[48] We hypothesized that due to the hydrophobic nature of various surface moieties on BSA[49] and its ability to adsorb to hydrophobic surfaces[44,50] such as carbon nanotubes, albumin could prevent nonspecific adsorption of uPA and serum proteins to the nanotube surface. To test this, we incubated a 50-fold excess by weight of BSA with the sensor for 30 min on ice prior to challenge with uPA. Initially tested in PBS, the sensor was then incubated with increasing concentrations of uPA in triplicate and fluorescence emission measured as above. We again found a monotonic red-shift with increasing uPA concentrations between 0.1 and 25 nM; however, the maximum shift increased greater than 2-fold to 3.5 nm for the (9,4) chirality (Figure 3A) and exhibited similar responses upon observation of the (8,6), and (8,7) chiralities, with red-shifts up to 4.1 and 4.7 nm, respectively (Figure S3C,D). We also found an extremely low LOD of 100 pM in buffer, the lowest concentration tested (Figure 2B), with a K_d of 5.95 nM (Figure S1B). These numbers were 500-fold lower for the LOD and 16.8-fold lower for K_d as compared to measurements in buffer without surface passivation. We attribute this large enhancement to the excess albumin allowing for coverage of the exposed nanotube surface and preventing uPA from nonspecifically binding to the nanotube and thus altering the emission response. This allowed for the very high affinity of antibody−uPA interaction to control the interaction of sensor complex and analyte, bringing uPA close to the surface of the nanotube in a controlled, consistent manner, enhancing sensor function and output.

Given the improved sensor functionality found in buffer following albumin passivation, we tested this construct in 10% FBS to again simulate the complex environment found in vivo. While the response was not as optimal as in buffer alone due to interferent protein and small molecule adsorption on the nanotube, we again found marked sensor improvement with BSA passivation. We found sensor red-shifting with a maximum of 1.6 nm, 33% more than without passivation (Figure 3B; compared to Figure 2B). Similarly, the (8,6) chirality shifted up to 1.5 nm with a K_d of 30 nM and the (8,7) chirality shifted 2.1 nm with a K_d of 40.8 nM (Figure S3C,D). We found a limit of detection of 25 nM and a K_d of 43.99 nM (Figure S1D). These represent improvements of 2-fold in LOD and 25% in K_d. Importantly, this red-shift is in contrast to the complete lack of response when passivated DNA-encapsulated nanotubes without the antibody were challenged with 100 nM uPA in serum (Figure S4). This experiment confirms that the functionality of the sensor is imparted by the specificity of the antibody for uPA. Sensor responses to all concentrations above the limit-of-detection were relatively stable from initial measurement up to 60 min (Figure S5). Improved sensing with BSA passivation was primarily observed for all three chiralities investigated (SI Table 1). We therefore attribute these results to both the increased sensitivity as explained above, but also a reduction in adsorption of nonspecific serum proteins and other interferents to the nanotube surface (Figure 3C). This allows for a more consistent sensor response due a reduction in competing surface signals from heterogeneous protein adsorption.

Finally, we used the enhanced specificity and sensitivity of the sensor to investigate its ability to detect uPA spiked into human blood products We found no significant difference in sensor red-shifting following 100 nM uPA addition to FBS, human serum, or human EDTA plasma (Figure 4A). We initially took the spectra of the albumin-passivated sensor in a solution of 10% whole blood, then spiked in 100 nM uPA. In this heterogeneous cellular and protein environment, we found a slight red-shift 60 min after addition of uPA (Figure S6A).

DOI: 10.1021/acssensors.8b00631
ACS Sens. 2018, 3, 1838−1845

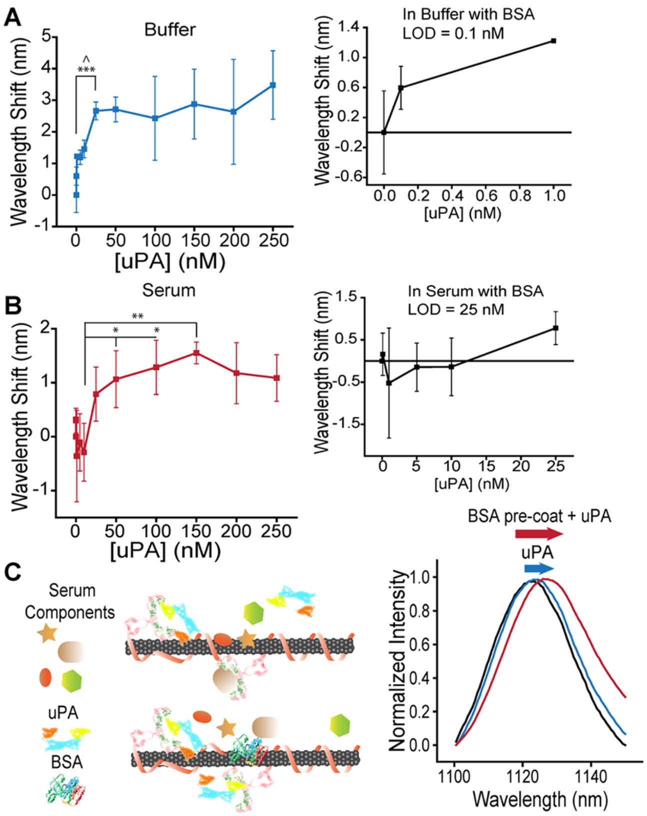

Figure 3. Antibody-SWCNT uPA sensor response after BSA precoating. (A) Change in BSA-coated sensor fluorescence emission center wavelength in PBS (positive value signifies a red-shift) as a function of uPA concentration for the (9,4) nanotube chirality. Two-sided one-way ANOVA with Tukey posthoc analysis performed to determine significance within the dynamic range of the sensor (0–25 nM): *** 0 nM and 25 nM ($p = 7.41 \times 10^{-6}$).^ indicates multiple significant comparisons not able to be shown due to proximity: 0 nM and 1 nM (* $p = 0.015$); 0 nM and 5 nM (** $p = 0.0084$); 0 nM and 10 nM (** $p = 0.0018$); 0.1 nM and 25 nM (*** $p = 8.59 \times 10^{-5}$); 1 nM and 25 nM (** $p = 0.0048$); 5 nM and 25 nM (** $p = 0.0017$); 10 nM and 25 nM (** $p = 0.0077$); other comparisons are not significant. (B) Change in BSA-coated sensor fluorescence emission center wavelength in PBS as a function of uPA concentration added for the (9,4) nanotube chirality. Two-sided one-way ANOVA with Tukey posthoc analysis performed to determine the significance within the dynamic range of the sensor (10–150 nM): ** 10 nM and 150 nM ($p = 0.0051$); * 10 nM and 100 nM ($p = 0.015$); * 10 nM and 50 nM ($p = 0.035$); other comparisons are not significant. Points represent the mean ± SD of three experiments. The low-concentration region on the left is magnified on the right to elucidate the limit of detection of the sensor under these conditions. (C) Schematic of uPA binding to the antibody nanotube complex in the absence or presence of BSA precoating with serum components in the solution. To the right are representative spectra from sensor alone (black), uPA-bound sensor (blue), and BSA precoated sensor bound to uPA (red).

We next tested sensor response over time in two human plasma preparations and human serum. In EDTA plasma, we found that 30 min after addition of 100 nM uPA, there was a slight quantifiable and consistent red-shift, which plateaued at 90 min, reaching a maximum of 1.19 nm (Figure 4B). In human serum we again found a consistent red-shift after 30 min of incubating the sensor with 100 nM uPA which reached a plateau around 90 min (Figure 4B) with a maximum of 0.98 nm. After adding 100 nM uPA to the passivated sensor incubated in 10% heparinized human plasma, we found some red-shifting at each time point, though there was significant variability in the measurements (Figure S6B). This result was expected due to the strong binding of heparin to uPA,[51,52] which clearly affects antibody binding and consistent sensing. A similar trend was found for each nanotube chirality investigated (Figure S7).

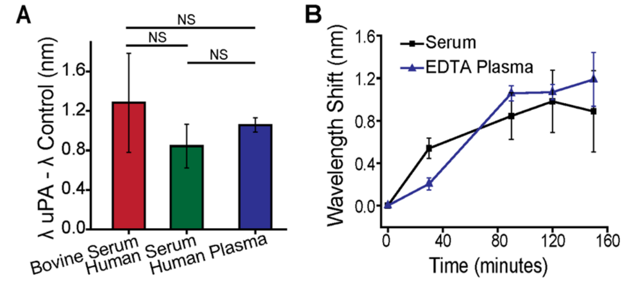

Figure 4. Sensor detection of uPA in human blood products. (A) Comparison of the change in center wavelength after addition of 100 nM uPA in bovine serum, human serum, and EDTA human plasma. Bars represent the mean ± of three experiments. Sensor wavelength difference between experiments and statistical analysis: bovine serum and human serum (0.44 nm; $p = 0.48$); bovine serum and human plasma (0.23 nm; $p = 0.86$); human serum and human plasma (0.21 nm; $p = 0.88$); two-sided one-way ANOVA with Tukey posthoc analysis, $p > 0.05$ was considered Not Significant (NS). (B) Change in sensor fluorescence emission center wavelength as a result of addition of 100 nM uPA over time compared to sensor without uPA added in 10% human EDTA plasma and 10% human serum. Points represent the mean ± SD of three experiments.

Further studies are necessary prior to the clinical translation of the sensor presented here as a point-of-care diagnostic tool. Current uPA detection in the clinic is performed by clinical laboratory enzyme-linked immunosorbent assays (ELISA) that may take hours and specialized equipment or training equipment to complete.[53] We expect that, following blood collection, we should be able to achieve sensitive biomarker detection within 15 min based on kinetics performed here. Additionally, serum uPA levels may range up to 17 nM, which our LOD in serum approaches.[17] To further increase the limit of detection of our sensor, future work may investigate exacerbating the optical bandgap modulation via chiral nanotube separation,[54−56] site-directed antibody conjugation,[57−60] and increasing antibody binding sites by using multivalent polymers instead of terminal-functionalized ssDNA.[41] In addition, brighter nanotubes may allow for greater sensitivity and sensor dynamic range.[36,61,62] Each of these future directions will ensure the ability to detect lower concentrations of uPA in biofluids from patient samples more representative of the range of clinical uPA concentrations.[18] Should long-term antibody functionality present a hurdle to translation, we expect future work will develop sensors with more stable sensing elements such as single-chain variable fragments (scFv) or nanobodies,[61,63−65] or aptamers[66−69] for prostate cancer biomarkers. The long-term functionality of this sensor in complex biological media will allow for repeated stable measurement of protein biomarkers in patient samples and in vivo.

The near-infrared fluorescent properties of this sensor and the mechanism of optical bandgap modulation may enable translation of this sensor as an in vivo tool for protein biomarker detection. In vivo imaging studies have used nanotube fluorescence to image vasculature in live animals

DOI: 10.1021/acssensors.8b00631
ACS Sens. 2018, 3, 1838−1845

and as intraoperative imaging probes.[70,71] Other studies have used the optical properties of nanotubes to detect protein biomarkers,[39] microRNA,[36] and nitric oxide in live animals.[72] The work we have presented here makes use of specific antibody–analyte interaction and nanotube optical bandgap modulation to achieve sensing. We also used sensor surface passivation with BSA to reduce the interferent effects of serum components found in vivo. To reduce interferent effects of cellular components in vivo, it is possible to protect the sensor using various strategies. The above-referenced works used implantation of nanotubes immobilized in a semipermeable membrane or hydrogel matrix to achieve this purpose and detect the desired analyte.[36,39,72] We therefore foresee future work in extending the sensing properties we have presented here to live mice and, eventually, to detection of metastatic prostate cancer in human patients. This sensor may be deployed to detect uPA in a cumulative manner to improve the limit of detection, discussed above.

In this work, we focused on the detection of the metastatic prostate cancer biomarker urokinase plasminogen activator. We envision that this type of sensor may enhance the specificity and sensitivity of traditional PSA-based testing. However, future work could develop a multiplexed biomarker sensing panel[36] using physical[73,74] or chiral[54−56] separation of nanotube-based sensors to detect uPA and other prostate cancer biomarkers such as prostate-specific antigen, prostate-specific membrane antigen, soluble uPA receptor, and various other proteins.[75,76] Thus, we imagine a rapid, real-time sensor for the detection of a panel of prostate cancer biomarkers.

■ CONCLUSIONS

We synthesized, characterized, and optimized a sensor for the metastatic prostate cancer biomarker uPA. We performed experiments to increase the sensitivity and functionality of the sensor in serum and demonstrated the potential of this sensor for uPA detection in various human blood products, potentiating future investigation into the clinical translation of this sensor. Studies to maximize sensor response and signal, develop multiplexed functionality, and translate in vivo and ex vivo bedside response remain prior to development of a clinical device. We expect this work to be a valuable tool in the rapid differentiation of indolent versus aggressive prostate cancer, thereby reducing overdiagnoses and overtreatment of this disease.

■ ASSOCIATED CONTENT

Supporting Information

The Supporting Information is available free of charge on the ACS Publications website at DOI: 10.1021/acssensors.8b00631.

> Change in sensor fluorescence center wavelength as a function of uPA concentration; response of additional nanotube chiralities; response of SWCNT with no antibody to uPA; kinetics of fluorescence center wavelength change; response of the sensor in additional human blood products; response of additional nanotube chiralities in human blood products; sensor characteristics for each nanotube chirality investigated under each given condition (PDF)

■ AUTHOR INFORMATION

Corresponding Author

*E-mail: hellerd@mskcc.org.

ORCID

Ryan M. Williams: 0000-0002-2381-8732

Daniel A. Heller: 0000-0002-6866-0000

Notes

The authors declare no competing financial interest.

■ ACKNOWLEDGMENTS

This work was supported by the NIH New Innovator Award (DP2-HD075698), the NIH Cancer Center Support Grant (P30 CA008748), the National Science Foundation CAREER Award (1752506), the Honorable Tina Brozman Foundation for Ovarian Cancer Research, the American Cancer Society, the Pershing Square Sohn Cancer Research Alliance, the Expect Miracles Foundation - Financial Services Against Cancer, the Louis V. Gerstner Jr. Young Investigator's Fund, the Frank A. Howard Scholars Program, the Alan and Sandra Gerry Metastasis Research Initiative, the Center for Molecular Imaging and Nanotechnology at Memorial Sloan Kettering Cancer Center, Cycle for Survival, the Anna Fuller Fund, Mr. William H. Goodwin and Mrs. Alice Goodwin and the Commonwealth Foundation for Cancer Research, the Imaging and Radiation Sciences Program, and the Experimental Therapeutics Center at Memorial Sloan Kettering Cancer Center. RMW was supported in part by the Ovarian Cancer Research Fund [Ann Schreiber Mentored Investigator Award 370463] and the American Heart Association [Postdoctoral Fellowship Award 17POST33650043]. The authors would like to thank M. Fleisher and K. Thoren for providing human blood products, P. Jena and D. Roxbury for instrument automation and MATLAB code, as well as helpful discussions, and J. Budhathoki-Uprety, Y. Shamay, R. Frederiksen, J. Harvey, and T. Galassi for helpful discussions.

■ REFERENCES

(1) Siegel, R. L.; Miller, K. D.; Jemal, A. Cancer statistics, 2016. *Ca-Cancer J. Clin.* **2016**, *66* (1), 7−30.

(2) Halpern, J. A.; Shoag, J. E.; Mittal, S.; Oromendia, C.; Ballman, K. V.; Hershman, D. L.; Wright, J. D.; Shih, Y.-C. T.; Nguyen, P. L.; Hu, J. C. Prognostic Significance of Digital Rectal Examination and Prostate Specific Antigen in the Prostate, Lung, Colorectal and Ovarian (PLCO) Cancer Screening Arm. *J. Urol.* **2017**, *197* (2), 363−368.

(3) Woolf, S. H. Screening for prostate cancer with prostate-specific antigen—an examination of the evidence. *N. Engl. J. Med.* **1995**, *333* (21), 1401−1405.

(4) Moyer, V. A. Screening for ovarian cancer: US Preventive Services Task Force reaffirmation recommendation statement. *Ann. Intern. Med.* **2012**, *157* (12), 900−904.

(5) Thompson, I. M.; Chi, C.; Ankerst, D. P.; Goodman, P. J.; Tangen, C. M.; Lippman, S. M.; Lucia, M. S.; Parnes, H. L.; Coltman, C. A., Jr. Effect of finasteride on the sensitivity of PSA for detecting prostate cancer. *Journal of the National Cancer Institute* **2006**, *98* (16), 1128−33.

(6) McGinley, K. F.; McMahon, G. C.; Brown, G. A. Impact of the US Preventive Services Task Force Grade D recommendation: assessment of evaluations for elevated prostate-specific antigen and prostate biopsies in a large urology group practice following statement revision. *Reviews in urology* **2015**, *17* (3), 171−177.

(7) Jemal, A.; Fedewa, S. A.; Ma, J.; Siegel, R.; Lin, C. C.; Brawley, O.; Ward, E. M. Prostate cancer incidence and PSA testing patterns in

DOI: 10.1021/acssensors.8b00631
ACS Sens. 2018, 3, 1838−1845

relation to USPSTF screening recommendations. *Jama* **2015**, *314* (19), 2054−2061.
(8) Draisma, G.; Etzioni, R.; Tsodikov, A.; Mariotto, A.; Wever, E.; Gulati, R.; Feuer, E.; de Koning, H. Lead time and overdiagnosis in prostate-specific antigen screening: importance of methods and context. *J. Natl. Cancer Inst.* **2009**, *101* (6), 374−383.
(9) Steyerberg, E.; Roobol, M.; Kattan, M.; Van der Kwast, T.; De Koning, H.; Schröder, F. Prediction of indolent prostate cancer: validation and updating of a prognostic nomogram. *J. Urol.* **2007**, *177* (1), 107−112.
(10) Loeb, S.; Bjurlin, M. A.; Nicholson, J.; Tammela, T. L.; Penson, D. F.; Carter, H. B.; Carroll, P.; Etzioni, R. Overdiagnosis and overtreatment of prostate cancer. *Eur. Urol.* **2014**, *65* (6), 1046−1055.
(11) Klotz, L. Prostate cancer overdiagnosis and overtreatment. *Curr. Opin. Endocrinol., Diabetes Obes.* **2013**, *20* (3), 204−209.
(12) Esserman, L. J.; Thompson, I. M.; Reid, B.; Nelson, P.; Ransohoff, D. F.; Welch, H. G.; Hwang, S.; Berry, D. A.; Kinzler, K. W.; Black, W. C.; et al. Addressing overdiagnosis and overtreatment in cancer: a prescription for change. *Lancet Oncol.* **2014**, *15* (6), e234−e242.
(13) Harbeck, N.; Schmitt, M.; Vetter, M.; Krol, J.; Paepke, D.; Uhlig, M.; Paepke, S.; Jänicke, F.; Geurts-Moespot, A.; von Minckwitz, G.; et al. Prospective biomarker trials Chemo N0 and NNBC-3 Europe validate the clinical utility of invasion markers uPA and PAI-1 in node-negative breast cancer. *Breast Care* **2008**, *3*, 11−15.
(14) Duffy, M.; Duggan, C. The urokinase plasminogen activator system: a rich source of tumour markers for the individualised management of patients with cancer. *Clin. Biochem.* **2004**, *37* (7), 541−548.
(15) Harris, L.; Fritsche, H.; Mennel, R.; Norton, L.; Ravdin, P.; Taube, S.; Somerfield, M. R.; Hayes, D. F.; Bast, R. C. American Society of Clinical Oncology 2007 update of recommendations for the use of tumor markers in breast cancer. *J. Clin. Oncol.* **2007**, *25* (33), 5287−5312.
(16) Saadoun, H.; Lamy, P.-J.; Thezenas, S.; Pouderoux, S.; Bibeau, F.; Montels, F.; Romieu, G.; Colombo, P.-E.; Gutowski, M.; Jacot, W. Prognostic impact of the inclusion of uPA/PAI-1 tumor levels in the current adjuvant treatment decision-making for early breast cancer. *Future Oncol.* **2014**, *10* (2), 195−209.
(17) Miyake, H.; Hara, I.; Yamanaka, K.; Gohji, K.; Arakawa, S.; Kamidono, S. Elevation of serum levels of urokinase-type plasminogen activator and its receptor is associated with disease progression and prognosis in patients with prostate cancer. *Prostate* **1999**, *39* (2), 123−129.
(18) Shariat, S. F.; Roehrborn, C. G.; McConnell, J. D.; Park, S.; Alam, N.; Wheeler, T. M.; Slawin, K. M. Association of the circulating levels of the urokinase system of plasminogen activation with the presence of prostate cancer and invasion, progression, and metastasis. *J. Clin. Oncol.* **2007**, *25* (4), 349−355.
(19) Duffy, M. Urokinase-type plasminogen activator: a potent marker of metastatic potential in human cancers. *Biochem. Soc. Trans.* **2002**, *30* (2), 207−210.
(20) Li, M.; Cushing, S. K.; Zhang, J.; Suri, S.; Evans, R.; Petros, W. P.; Gibson, L. F.; Ma, D.; Liu, Y.; Wu, N. Three-Dimensional Hierarchical Plasmonic Nano-Architecture Enhanced Surface-Enhanced Raman Scattering Immuno-Sensor for Cancer Biomarker Detection in Blood Plasma. *ACS Nano* **2013**, *7* (6), 4967.
(21) Uludag, Y.; Tothill, I. E. Cancer biomarker detection in serum samples using surface plasmon resonance and quartz crystal microbalance sensors with nanoparticle signal amplification. *Anal. Chem.* **2012**, *84* (14), 5898−5904.
(22) Yu, X.; Munge, B.; Patel, V.; Jensen, G.; Bhirde, A.; Gong, J. D.; Kim, S. N.; Gillespie, J.; Gutkind, J. S.; Papadimitrakopoulos, F. Carbon nanotube amplification strategies for highly sensitive immunodetection of cancer biomarkers. *J. Am. Chem. Soc.* **2006**, *128* (34), 11199.
(23) Ji, S.-r.; Liu, C.; Zhang, B.; Yang, F.; Xu, J.; Long, J.; Jin, C.; Fu, D.-l.; Ni, Q.-x.; Yu, X.-j. Carbon nanotubes in cancer diagnosis and therapy. *Biochim. Biophys. Acta, Rev. Cancer* **2010**, *1806* (1), 29−35.
(24) Welsher, K.; Sherlock, S. P.; Dai, H. Deep-tissue anatomical imaging of mice using carbon nanotube fluorophores in the second near-infrared window. *Proc. Natl. Acad. Sci. U. S. A.* **2011**, *108* (22), 8943−8948.
(25) Yi, H.; Ghosh, D.; Ham, M.-H.; Qi, J.; Barone, P. W.; Strano, M. S.; Belcher, A. M. M13 phage-functionalized single-walled carbon nanotubes as nanoprobes for second near-infrared window fluorescence imaging of targeted tumors. *Nano Lett.* **2012**, *12* (3), 1176.
(26) Hong, G.; Lee, J. C.; Robinson, J. T.; Raaz, U.; Xie, L.; Huang, N. F.; Cooke, J. P.; Dai, H. Multifunctional in vivo vascular imaging using near-infrared II fluorescence. *Nat. Med.* **2012**, *18* (12), 1841−1846.
(27) Heller, D. A.; Baik, S.; Eurell, T. E.; Strano, M. S. Single-walled carbon nanotube spectroscopy in live cells: towards long-term labels and optical sensors. *Adv. Mater.* **2005**, *17* (23), 2793−2799.
(28) Schäfer, S.; Cogan, N. M.; Krauss, T. D. Spectroscopic investigation of electrochemically charged individual (6, 5) single-walled carbon nanotubes. *Nano Lett.* **2014**, *14* (6), 3138−3144.
(29) Choi, J. H.; Strano, M. S. Solvatochromism in single-walled carbon nanotubes. *Appl. Phys. Lett.* **2007**, *90* (22), 223114.
(30) Heller, D. A.; Pratt, G. W.; Zhang, J.; Nair, N.; Hansborough, A. J.; Boghossian, A. A.; Reuel, N. F.; Barone, P. W.; Strano, M. S. Peptide secondary structure modulates single-walled carbon nanotube fluorescence as a chaperone sensor for nitroaromatics. *Proc. Natl. Acad. Sci. U. S. A.* **2011**, *108* (21), 8544−8549.
(31) Heller, D. A.; Jin, H.; Martinez, B. M.; Patel, D.; Miller, B. M.; Yeung, T.-K.; Jena, P. V.; Höbartner, C.; Ha, T.; Silverman, S. K. Multimodal optical sensing and analyte specificity using single-walled carbon nanotubes. *Nat. Nanotechnol.* **2009**, *4* (2), 114−120.
(32) Heller, D. A.; Jeng, E. S.; Yeung, T.-K.; Martinez, B. M.; Moll, A. E.; Gastala, J. B.; Strano, M. S. Optical detection of DNA conformational polymorphism on single-walled carbon nanotubes. *Science* **2006**, *311* (5760), 508−511.
(33) Jena, P. V.; Roxbury, D.; Galassi, T. V.; Akkari, L.; Horoszko, C. P.; Iaea, D. B.; Budhathoki-Uprety, J.; Pipalia, N.; Haka, A. S.; Harvey, J. D.; et al. A carbon nanotube optical reporter maps endolysosomal lipid flux. *ACS Nano* **2017**, *11* (11), 10689−10703.
(34) Roxbury, D.; Jena, P. V.; Shamay, Y.; Horoszko, C. P.; Heller, D. A. Cell Membrane Proteins Modulate the Carbon Nanotube Optical Bandgap via Surface Charge Accumulation. *ACS Nano* **2016**, *10* (1), 499−506.
(35) Budhathoki-Uprety, J.; Langenbacher, R. E.; Jena, P. V.; Roxbury, D.; Heller, D. A. A Carbon Nanotube Optical Sensor Reports Nuclear Entry via a Noncanonical Pathway. *ACS Nano* **2017**, *11* (4), 3875−3882.
(36) Harvey, J. D.; Jena, P. V.; Baker, H. A.; Zerze, G. H.; Williams, R. M.; Galassi, T. V.; Roxbury, D.; Mittal, J.; Heller, D. A. A carbon nanotube reporter of microRNA hybridization events in vivo. *Nature Biomedical Engineering* **2017**, *1*, 0041.
(37) Harvey, J. D.; Baker, H. A.; Mercer, E.; Budhathoki-Uprety, J.; Heller, D. A. Control of Carbon Nanotube Solvatochromic Response to Chemotherapeutic Agents. *ACS Appl. Mater. Interfaces* **2017**, *9* (43), 37947−37953.
(38) Zhang, J.; Kruss, S.; Hilmer, A. J.; Shimizu, S.; Schmois, Z.; De La Cruz, F.; Barone, P. W.; Reuel, N. F.; Heller, D. A.; Strano, M. S. A Rapid, Direct, Quantitative, and Label-Free Detector of Cardiac Biomarker Troponin T Using Near-Infrared Fluorescent Single-Walled Carbon Nanotube Sensors. *Adv. Healthcare Mater.* **2014**, *3* (3), 412−423.
(39) Williams, R. M.; Lee, C.; Galassi, T. V.; Harvey, J. D.; Leicher, R.; Sirenko, M.; Dorso, M. A.; Shah, J.; Olvera, N.; Dao, F.; et al. Noninvasive ovarian cancer biomarker detection via an optical nanosensor implant. *Science advances* **2018**, *4* (4), eaaq1090.
(40) Roxbury, D.; Jena, P. V.; Williams, R. M.; Enyedi, B.; Niethammer, P.; Marcet, S.; Verhaegen, M.; Blais-Ouellette, S.;

DOI: 10.1021/acssensors.8b00631
ACS Sens. 2018, 3, 1838−1845

Heller, D. A. Hyperspectral Microscopy of Near-Infrared Fluorescence Enables 17-Chirality Carbon Nanotube Imaging. *Sci. Rep.* **2015**, *5*, 1 DOI: 10.1038/srep14167.
(41) Budhathoki-Uprety, J.; Jena, P. V.; Roxbury, D.; Heller, D. A. Helical polycarbodiimide cloaking of carbon nanotubes enables internanotube exciton energy transfer modulation. *J. Am. Chem. Soc.* **2014**, *136* (44), 15545−15550.
(42) Rossi, N. E.; Reiné, J.; Pineda-Lezamit, M.; Pulgar, M.; Meza, N. W.; Swamy, M.; Risueno, R.; Schamel, W. W.; Bonay, P.; Fernández-Malavé, E. Differential antibody binding to the surface $\alpha\beta$TCR· CD3 complex of CD4+ and CD8+ T lymphocytes is conserved in mammals and associated with differential glycosylation. *Int. Immunol.* **2008**, *20* (10), 1247−1258.
(43) Brown, E. P.; Weiner, J. A.; Lin, S.; Natarajan, H.; Normandin, E.; Barouch, D. H.; Alter, G.; Sarzotti-Kelsoe, M.; Ackerman, M. E. Optimization and qualification of an Fc Array assay for assessments of antibodies against HIV-1/SIV. *J. Immunol. Methods* **2018**, *455*, 24−33.
(44) Budhathoki-Uprety, J.; Harvey, J. D.; Isaac, E.; Williams, R. M.; Galassi, T. V.; Langenbacher, R. E.; Heller, D. A. Polymer cloaking modulates the carbon nanotube protein corona and delivery into cancer cells. *J. Mater. Chem. B* **2017**, *5* (32), 6637−6644.
(45) Barua, S.; Yoo, J.-W.; Kolhar, P.; Wakankar, A.; Gokarn, Y. R.; Mitragotri, S. Particle shape enhances specificity of antibody-displaying nanoparticles. *Proc. Natl. Acad. Sci. U. S. A.* **2013**, *110* (9), 3270−3275.
(46) Williams, R. M.; Shah, J.; Ng, B. D.; Minton, D. R.; Gudas, L. J.; Park, C. Y.; Heller, D. A. Mesoscale Nanoparticles Selectively Target the Renal Proximal Tubule Epithelium. *Nano Lett.* **2015**, *15* (4), 2358−2364.
(47) Spraggon, G.; Phillips, C.; Nowak, U. K.; Ponting, C. P.; Saunders, D.; Dobson, C. M.; Stuart, D. I.; Jones, E. Y. The crystal structure of the catalytic domain of human urokinase-type plasminogen activator. *Structure* **1995**, *3* (7), 681−691.
(48) Sweryda-Krawiec, B.; Devaraj, H.; Jacob, G.; Hickman, J. J. A new interpretation of serum albumin surface passivation. *Langmuir* **2004**, *20* (6), 2054−2056.
(49) Haskard, C. A.; Li-Chan, E. C. Hydrophobicity of bovine serum albumin and ovalbumin determined using uncharged (PRODAN) and anionic (ANS-) fluorescent probes. *J. Agric. Food Chem.* **1998**, *46* (7), 2671−2677.
(50) Jeyachandran, Y.; Mielczarski, E.; Rai, B.; Mielczarski, J. Quantitative and qualitative evaluation of adsorption/desorption of bovine serum albumin on hydrophilic and hydrophobic surfaces. *Langmuir* **2009**, *25* (19), 11614−11620.
(51) Andrade-Gordon, P.; Strickland, S. Interaction of heparin with plasminogen activators and plasminogen: effects on the activation of plasminogen. *Biochemistry* **1986**, *25* (14), 4033−4040.
(52) Kenagy, R. D.; Clowes, A. W. Regulation of baboon arterial smooth muscle cell plasminogen activators by heparin and growth factors. *Thromb. Res.* **1995**, *77* (1), 55−61.
(53) Duffy, M. J.; McGowan, P. M.; Harbeck, N.; Thomssen, C.; Schmitt, M. uPA and PAI-1 as biomarkers in breast cancer: validated for clinical use in level-of-evidence-1 studies. *Breast Cancer Res.* **2014**, *16* (4), 428.
(54) Tu, X.; Manohar, S.; Jagota, A.; Zheng, M. DNA sequence motifs for structure-specific recognition and separation of carbon nanotubes. *Nature* **2009**, *460* (7252), 250−253.
(55) Zheng, M.; Jagota, A.; Semke, E. D.; Diner, B. A.; McLean, R. S.; Lustig, S. R.; Richardson, R. E.; Tassi, N. G. DNA-assisted dispersion and separation of carbon nanotubes. *Nat. Mater.* **2003**, *2* (5), 338−342.
(56) Khripin, C. Y.; Fagan, J. A.; Zheng, M. Spontaneous partition of carbon nanotubes in polymer-modified aqueous phases. *J. Am. Chem. Soc.* **2013**, *135* (18), 6822−6825.
(57) Zeglis, B. M.; Davis, C. B.; Aggeler, R.; Kang, H. C.; Chen, A.; Agnew, B. J.; Lewis, J. S. Enzyme-mediated methodology for the site-specific radiolabeling of antibodies based on catalyst-free click chemistry. *Bioconjugate Chem.* **2013**, *24* (6), 1057−1067.
(58) Junutula, J. R.; Raab, H.; Clark, S.; Bhakta, S.; Leipold, D. D.; Weir, S.; Chen, Y.; Simpson, M.; Tsai, S. P.; Dennis, M. S.; et al. Site-specific conjugation of a cytotoxic drug to an antibody improves the therapeutic index. *Nat. Biotechnol.* **2008**, *26* (8), 925−932.
(59) Rodwell, J. D.; Alvarez, V. L.; Lee, C.; Lopes, A. D.; Goers, J.; King, H. D.; Powsner, H. J.; McKearn, T. J. Site-specific covalent modification of monoclonal antibodies: in vitro and in vivo evaluations. *Proc. Natl. Acad. Sci. U. S. A.* **1986**, *83* (8), 2632−2636.
(60) Behrens, C. R.; Liu, B. In *Methods for site-specific drug conjugation to antibodies, Mabs*; Landes Bioscience: 2013; pp 46−53.
(61) Piao, Y.; Meany, B.; Powell, L. R.; Valley, N.; Kwon, H.; Schatz, G. C.; Wang, Y. Brightening of carbon nanotube photoluminescence through the incorporation of sp3 defects. *Nat. Chem.* **2013**, *5* (10), 840−845.
(62) Campo, J.; Piao, Y.; Lam, S.; Stafford, C.; Streit, J.; Simpson, J.; Walker, A. H.; Fagan, J. Enhancing single-wall carbon nanotube properties through controlled endohedral filling. *Nanoscale Horizons* **2016**, *1* (4), 317−324.
(63) Williams, R. M.; Hajiran, C. J.; Nayeem, S.; Sooter, L. J. Identification of an antibody fragment specific for androgen-dependent prostate cancer cells. *BMC Biotechnol.* **2014**, *14* (1), 81.
(64) Muyldermans, S. Nanobodies: natural single-domain antibodies. *Annu. Rev. Biochem.* **2013**, *82*, 775−797.
(65) Williams, R. M.; Sooter, L. J. In vitro selection of cancer cell-specific molecular recognition elements from amino acid libraries. *J. Immunol. Res.* **2015**, *2015*, 186586.
(66) Tuerk, C.; Gold, L. Systematic evolution of ligands by exponential enrichment: RNA ligands to bacteriophage T4 DNA polymerase. *Science* **1990**, *249* (4968), 505−10.
(67) Wang, G.; Wang, Y.; Chen, L.; Choo, J. Nanomaterial-assisted aptamers for optical sensing. *Biosens. Bioelectron.* **2010**, *25* (8), 1859−1868.
(68) Yang, R.; Tang, Z.; Yan, J.; Kang, H.; Kim, Y.; Zhu, Z.; Tan, W. Noncovalent assembly of carbon nanotubes and single-stranded DNA: an effective sensing platform for probing biomolecular interactions. *Anal. Chem.* **2008**, *80* (19), 7408−7413.
(69) Williams, R. M.; Nayeem, S.; Dolash, B. D.; Sooter, L. J. The effect of DNA-dispersed single-walled carbon nanotubes on the polymerase chain reaction. *PLoS One* **2014**, *9* (4), e94117.
(70) Hong, G.; Diao, S.; Chang, J.; Antaris, A. L.; Chen, C.; Zhang, B.; Zhao, S.; Atochin, D. N.; Huang, P. L.; Andreasson, K. I. Through-skull fluorescence imaging of the brain in a new near-infrared window. *Nat. Photonics* **2014**, *8* (9), 723−730.
(71) Ghosh, D.; Bagley, A. F.; Na, Y. J.; Birrer, M. J.; Bhatia, S. N.; Belcher, A. M. Deep, noninvasive imaging and surgical guidance of submillimeter tumors using targeted M13-stabilized single-walled carbon nanotubes. *Proc. Natl. Acad. Sci. U. S. A.* **2014**, *111* (38), 13948−13953.
(72) Iverson, N. M.; Barone, P. W.; Shandell, M.; Trudel, L. J.; Sen, S.; Sen, F.; Ivanov, V.; Atolia, E.; Farias, E.; McNicholas, T. P.; et al. In vivo biosensing via tissue-localizable near-infrared-fluorescent single-walled carbon nanotubes. *Nat. Nanotechnol.* **2013**, *8* (11), 873−880.
(73) Qi, P.; Vermesh, O.; Grecu, M.; Javey, A.; Wang, Q.; Dai, H.; Peng, S.; Cho, K. Toward large arrays of multiplex functionalized carbon nanotube sensors for highly sensitive and selective molecular detection. *Nano Lett.* **2003**, *3* (3), 347−351.
(74) Zheng, G.; Patolsky, F.; Cui, Y.; Wang, W. U.; Lieber, C. M. Multiplexed electrical detection of cancer markers with nanowire sensor arrays. *Nat. Biotechnol.* **2005**, *23* (10), 1294−1301.
(75) Williams, R.; Naz, R. Novel biomarkers and therapeutic targets for prostate cancer. *Front. Biosci., Scholar Ed.* **2009**, *2*, 677−684.
(76) Prensner, J. R.; Rubin, M. A.; Wei, J. T.; Chinnaiyan, A. M. Beyond PSA: the next generation of prostate cancer biomarkers. *Sci. Transl. Med.* **2012**, *4* (127), 127rv3−127rv3.

DOI: 10.1021/acssensors.8b00631
ACS Sens. 2018, 3, 1838−1845